

Subnanometre resolution in three-dimensional magnetic resonance imaging of individual dark spins

M. S. Grinolds¹, M. Warner¹, K. De Greve¹, Y. Dovzhenko¹, L. Thiel^{1,2}, R. L. Walsworth^{1,3}, S. Hong⁴, P. Maletinsky² and A. Yacoby^{1*}

Magnetic resonance imaging (MRI) has revolutionized biomedical science by providing non-invasive, three-dimensional biological imaging¹. However, spatial resolution in conventional MRI systems is limited to tens of micrometres², which is insufficient for imaging on molecular scales. Here, we demonstrate an MRI technique that provides subnanometre spatial resolution in three dimensions, with single electron-spin sensitivity. Our imaging method works under ambient conditions and can measure ubiquitous 'dark' spins, which constitute nearly all spin targets of interest. In this technique, the magnetic quantum-projection noise of dark spins is measured using a single nitrogen-vacancy (NV) magnetometer located near the surface of a diamond chip. The distribution of spins surrounding the NV magnetometer is imaged with a scanning magnetic-field gradient. To evaluate the performance of the NV-MRI technique, we image the three-dimensional landscape of electronic spins at the diamond surface and achieve an unprecedented combination of resolution (0.8 nm laterally and 1.5 nm vertically) and single-spin sensitivity. Our measurements uncover electronic spins on the diamond surface that can potentially be used as resources for improved magnetic imaging. This NV-MRI technique is immediately applicable to diverse systems including imaging spin chains, readout of spin-based quantum bits, and determining the location of spin labels in biological systems.

Magnetic resonance imaging (MRI) on the atomic scale would have wide-ranging applications, including determining the structure of individual biomolecules, imaging the dynamics of bottom-up molecular engineering³ and achieving site-resolved readout in solid-state quantum simulators⁴. Performing conventional MRI on submicrometre length scales is not possible because macroscopically generated magnetic-field gradients limit the spatial resolution, and inductive detection schemes suffer from significant thermal noise². Great progress has been made using scanning-probe-based magnetic gradient techniques, which enable nanoscale MRI^{5,6} using ultrasensitive force detection at cryogenic temperatures^{7,8} or fluorescence measurements from optically 'bright' spins such as nitrogen vacancy (NV) colour centres in diamond^{6,9}. However, for most MRI applications, measurements must be taken near room temperature, and nearly all targets of interest contain optically 'dark' spins that are unpolarized or weakly polarized. In this Letter we demonstrate a technique to perform three-dimensional MRI with subnanometre resolution on dark electronic spins under ambient conditions, using a single NV centre near the

surface of a diamond as a magnetic sensor of its local environment, together with a scanning-tip magnetic-field gradient to provide high spatial resolution. Our method is compatible with numerous developed methods for bringing imaging targets sufficiently close for NV magnetic detection^{10–16}, and extends the reach of nanoscale MRI to previously inaccessible systems in both the physical and life sciences.

The NV-MRI technique combines an NV magnetometer with scanning magnetic-field gradients using an atomic force microscope (Fig. 1a). Individual shallowly implanted NV centres (nominal depth of 10 nm) are placed in the focus of a confocal microscope so that the NV electronic spin can be initialized by optical pumping, used as a sensor to measure nearby dark spins via magnetic dipole–dipole interactions, and read out using time and spin-state dependent fluorescence¹⁷. To image the three-dimensional distribution of dark spins via NV-MRI, we apply a local magnetic-field gradient with a scanning magnetic tip. The magnetic tip provides a narrow spatial volume (a 'resonant slice') in which dark spins are on resonance with a driving radiofrequency (RF) field. Only dark spins within the resonant slice are RF-driven and thus contribute to the dark-spin magnetic signal measured by the NV centre. The three-dimensional position of the resonant slice is then controllably scanned throughout the sample with ångstrom precision by moving the magnetic tip, allowing high-resolution three-dimensional MRI of target dark spins.

To create three-dimensional magnetic resonance images, the detected NV-MRI signal at each magnetic tip position is made conditional on the resonant RF-driving of target dark spins via double electron–electron resonance (DEER)^{11,13,18,19}. As illustrated in Fig. 1b, microwave (MW) pulsing on the NV spin prepares a coherent superposition of NV-spin states with phase ϕ_{NV} that evolves with evolution time τ_{NV} in proportion to the local magnetic field (projected along the NV quantization axis) from the target dark spins (B_{Dark}). Halfway through τ_{NV} , simultaneous MW and RF π -pulses are applied to the NV and target dark spins, respectively, so that ϕ_{NV} accumulates only for resonant dark spins and refocuses for off-resonant dark spins. Target dark spins are in an unpolarized mixed state at room temperature, and so across multiple spin measurements, $\langle\phi_{\text{NV}}\rangle = 0$; however, DEER measures $\langle\cos(\phi_{\text{NV}})\rangle$, which is independent of the dark spins' initial states and consequently measures the variance of the dark spins (coming from magnetic quantum-projection noise).

When scanning the magnetic tip to perform NV-MRI, we simultaneously frequency-lock the applied MW signal to the NV spin

¹Department of Physics, Harvard University, 17 Oxford Street, Cambridge, Massachusetts 02138, USA, ²Department of Physics, University of Basel, Klingelbergstrasse 82, Basel, CH-4056 Switzerland, ³Harvard-Smithsonian Center for Astrophysics, 60 Garden Street, Cambridge, Massachusetts 02138, USA, ⁴Vienna Center for Quantum Science and Technology (VCQ), Faculty of Physics, University of Vienna, Boltzmanngasse 5, A-1090 Vienna, Austria.

*e-mail: yacoby@physics.harvard.edu

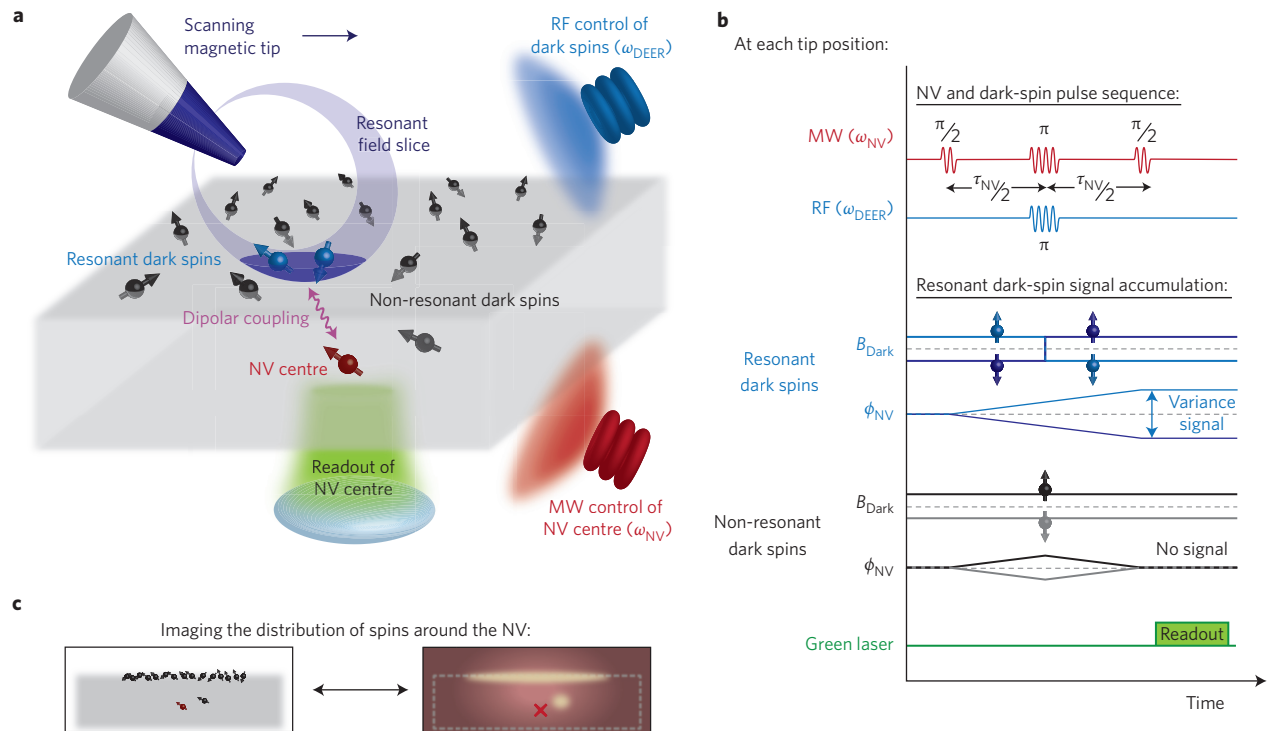


Figure 1 | Dark-spin MRI using scanning gradients and a single NV sensor. **a**, Schematic of the NV-MRI technique depicting an NV centre in diamond situated in a confocal laser spot with nearby dark spins. A scanning magnetic tip is placed within 100 nm of the diamond surface. Applied microwave (MW) and radiofrequency (RF) signals allow for independent coherent control of the NV spin and dark spins. By scanning the magnetic tip, non-resonant dark spins (shown in black) are systematically brought into resonance with the RF signal (resonant spins shown in blue) and are measured via optically detected magnetic resonance of the NV sensor. **b**, DEER pulse sequences executed at each magnetic tip position. A MW spin-echo sequence is executed on the NV sensor. By synchronizing a RF π pulse on the dark spins with the MW π pulse in the echo sequence, the time-varying magnetic field from the dark spins (B_{Dark}) in the resonant slice (light/dark blue) leads to net NV spin phase (ϕ_{NV}) accumulation, while the magnetic field from non-resonant dark (grey/black) spins is refocused and thus their effects on the NV spin are cancelled, irrespective of the initial polarization state of the dark spins. **c**, Cartoon of how NV-MRI provides three-dimensional mapping of the distribution of dark electronic spins near the NV sensor (indicated by the red cross), with subnanometre resolution (see main text for further discussion).

resonance²⁰, which keeps the NV sensor active and also measures the tip-induced frequency detuning. The resulting spatial map of the frequency-locked NV signal experimentally determines the point-spread function (PSF) for dark-spin imaging (Supplementary Fig. 5). Because dark spins are spatially offset from the NV location and/or distributed over a non-zero volume, the observed dark-spin signal as a function of magnetic tip position is offset and/or broadened from the measured PSF, and the dark-spin spatial distribution can be found via deconvolution (Fig. 1c). An important feature of our technique is that by directly measuring the dark-spin PSF there is no reliance on magnetic-field modelling or iterative deconvolution schemes that must be simultaneously solved for both an unknown signal and an unknown PSF.

The spatial resolution of NV-MRI is given by $1/(\tau\gamma|\nabla B_{\text{tip}}|)$, where γ and τ are the target spin's gyromagnetic ratio and spin-interrogation time, respectively, and ∇B_{tip} is the gradient of the tip's magnetic field at the target spin's position projected along the spin's quantization axis. We determined the spatial resolution limit in our set-up by measuring ∇B_{tip} using a single NV centre, with a relatively long T_2^* coherence time, which allows for a long τ (Fig. 2). Using a $\tau = 450$ ns Ramsey interferometry sequence, we measured spatial fringes with oscillation periods down to 3.3 ± 0.3 Å (Fig. 2a), showing that the magnetic tip produces a gradient of 2.4 G nm^{-1} and demonstrating that the experimental set-up is mechanically stable down to subnanometre length scales. By bringing the tip closer to the NV centre (Fig. 2b), we observed gradients of at least 12 G nm^{-1} (effective $\tau = 120$ ns);

however, vibrations in our experimental set-up currently limit the spatial resolution to 2.5 Å. For NV-MRI of dark spins with static tip gradients, the target spin interrogation time is limited by the target spin T_2^* (~ 150 ns), enabling subnanometre three-dimensional NV-MRI resolution.

To demonstrate such subnanometre NV-MRI performance, we spatially mapped the spin environment of individual NV centres near a diamond surface. Shallow NV centres are the mainstay for NV-based nanoscale sensing^{10–14,21–23} and quantum-information processing^{4,24}, yet their dominant sources of decoherence have not been identified and localized. In the absence of the magnetic tip, we first used DEER spectroscopy and observed a $g = 2$ dark electronic spin bath coupled to shallow NV spins, consistent with previous measurements on near-surface NV centres^{13,25,26}. We measured $g = 2$ electron-spin resonances for more than 60% of measured NV spins (>30 centres in three diamond samples; Supplementary Figs 1 and 2). Note that we can rule out these dark spins as being nitrogen P1 centres because their DEER spectroscopy contains a single resonance, in contrast to the multi-peaked resonance structure of P1 centres¹⁸.

We present NV-MRI imaging experiments mapping the spatial locations of these $g = 2$ dark spins around two separate NV centres by scanning the magnetic tip in three dimensions (Fig. 3). Comparing the measured dark-spin PSF to the observed dark-spin resonance slice (Fig. 3b and d, right panel), we find that for both NV centres the dark-spin signal is shifted vertically from the PSF, which shows that the imaged dark spins are located 10 nm and

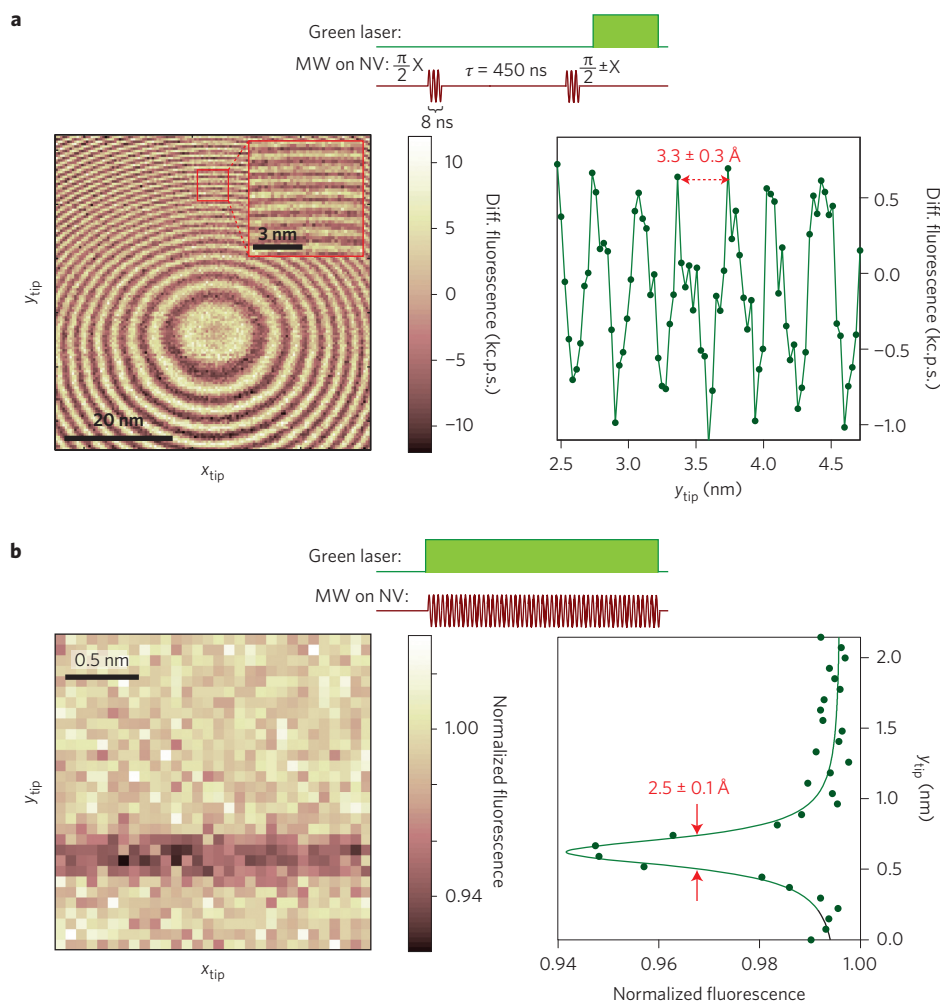


Figure 2 | Scanning gradients with subnanometre MRI resolution. a, Scanning Ramsey interferometry on a single, shallow NV centre in a 0.12 T external magnetic field. As the magnetic tip is scanned laterally over the NV centre 50 nm above the diamond surface and near the NV centre, the resultant variation in magnetic field at the NV centre leads to two-dimensional spatial oscillations in the measured NV Ramsey interferometry fluorescence signal as a function of lateral tip position (left panel). Plotted is the difference in fluorescence between two Ramsey sequences having a π phase shift between their readout pulses. A linecut along the y direction (30 nm above the diamond surface, right panel) shows oscillations with a period of 3.3 ± 0.3 Å, indicating that the tip-induced magnetic-field gradients are 2.4 G nm $^{-1}$. **b**, Continuous-wave ESR magnetometry with an inverse linewidth of $\tau = 120$ ns. Magnetic-tip scan with a 20 nm vertical offset from the NV (left panel), zoomed into one resonant slice with a full-width at half-maximum of 2.5 Å (right panel) and thus a 12 G nm $^{-1}$ tip-induced magnetic-field gradients.

14 nm above the two NV sensors, respectively (Fig. 3b,d). Given the implantation energy used to form the shallow NV spins, the observed dark-spin location is consistent with them being at the diamond surface (nominal depth of 10 ± 3 nm; Supplementary Methods).

An image deconvolution along the x - z plane (Fig. 3d) directly shows that the dark spin distribution is spread out in a line (vertical resolution of 1.5 nm limited by measurement noise and pixel size), indicating a layer of spins at the diamond surface. This layer of dark spins probably extends further in the x - z plane direction with near-uniform coverage over the diamond surface, but laterally distant spins couple more weakly to the single NV and are undetectable when their signal becomes smaller than the measurement noise. As we directly measure the vertical distance between the NV sensor and the dark-spin layer, the density of dark spins in the layer can be found using the dark-spin/NV coupling rate (~ 100 kHz for this NV centre)²². The extracted two-dimensional dark-spin density is 0.5 spins nm $^{-2}$, which for a surface layer corresponds to a single unpaired electron spin every ~ 60 surface atoms.

We also observed that some shallow NV spins are coherently coupled to an individual dark electronic spin, as indicated by

coherent oscillations in the DEER signal as a function of evolution time (Fig. 4a)²⁷ (Supplementary Fig. 6). We note that the intensity of the observed dark-spin DEER oscillations cannot be explained by a classical single spin, where the spin is modelled by a magnetic moment that can have an arbitrary, continuous magnetization. In that situation, for an unpolarized dark spin, the measured DEER signal would average over all possible magnetizations and the signal would decay to the NV mixed state. However, for an $S = 1/2$ quantum spin, measurement of its magnetization can only yield two values, giving single-frequency oscillations in the DEER signal, as we observe. This quantum-projection noise enhances the signal for MRI imaging, and in this case it increases the signal-to-noise of dark-spin imaging by 1.9 compared to a classical variance.

We next imaged the three-dimensional location of this coherently coupled dark spin by scanning the magnetic tip both laterally (Fig. 4b) and vertically (Fig. 4c) and using the deconvolution method described in Fig. 3. For vertical imaging, we found an offset of the dark-spin position relative to the NV sensor of $[\Delta y, \Delta z] = [5.1 \pm 0.3, -3.65 \pm 0.05]$ nm, where the errors indicate

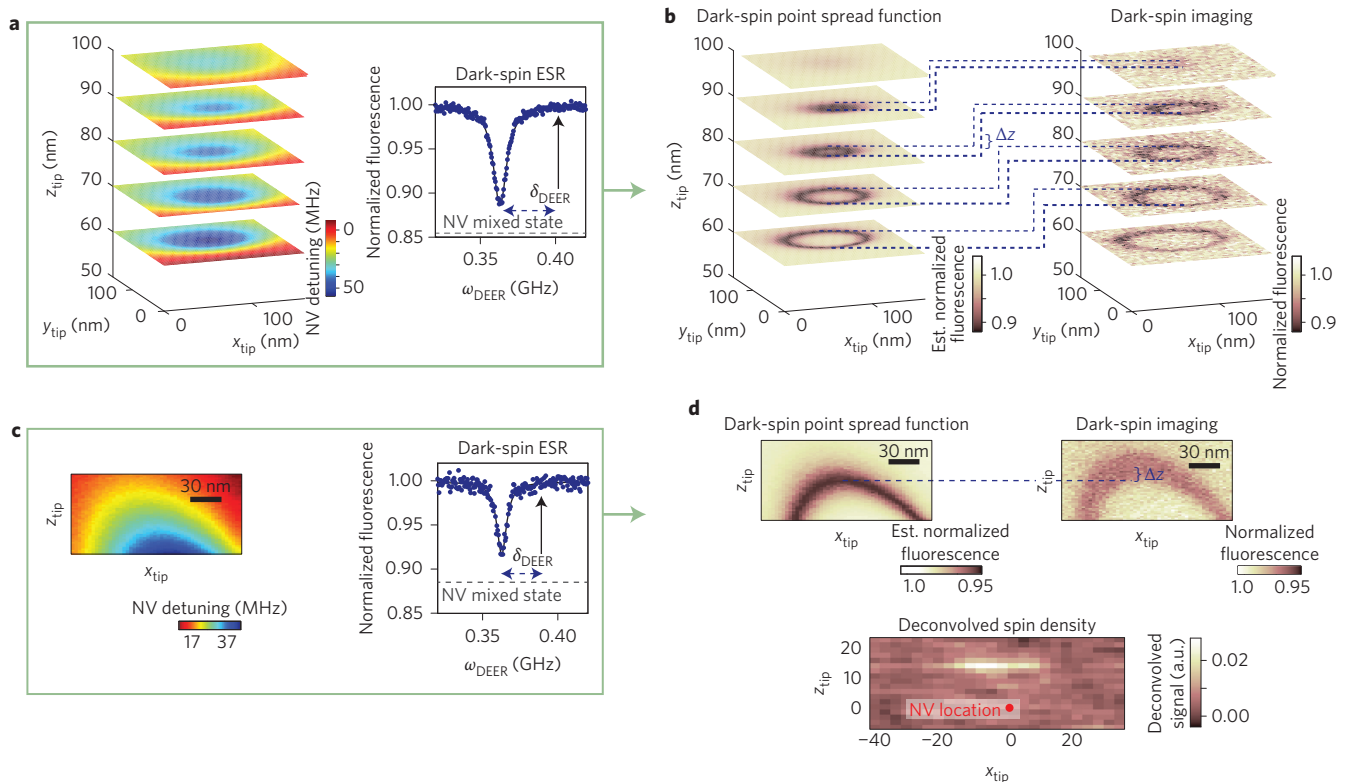


Figure 3 | MRI of ensembles of dark spins at the diamond surface. **a**, Determining the dark-spin NV-MRI PSF. Three-dimensional plot of the detuning of the frequency-locked NV microwave signal ω_{NV} , measured by xy scanning of the magnetic tip with variable z offset of 60 nm to 100 nm from the diamond surface (left). This detuning map is combined with the tip-independent dark-spin ESR spectrum (right) to determine the dark-spin PSF (Supplementary Fig. 5). **b**, NV-MRI tomography of dark spins proximal to an individual shallow NV centre. Displacement of the dark-spin resonance slice image (right) from the dark-spin PSF (left) indicates the location of the dark spins with respect to the NV centre. For a given dark-spin lateral (xy) image, the best match to the dark-spin PSF (determined from the diameter of the resonance circle) is shifted by $\Delta z = 0$ nm, showing that the dark spins lie at or very close to the diamond surface. **c**, Dark-spin PSF determination for a second NV centre in a vertical (xz) scan. **d**, Vertical (xz) NV-MRI of dark spins. Similar to **b**, the dark-spin resonance slice image is vertically shifted ($\Delta z = 4$ nm for this NV sensor), again suggestive of surface dark spins. Deconvolving the dark-spin image with the PSF gives the spatial distribution of the nearby dark spins, indicating a surface layer above the shallow NV centre.

the precision of the position determination (Supplementary Methods), with a spatial resolution of 1.5 ± 0.6 nm given by the spatial width of the dark-spin resonance. For lateral imaging, the dark-spin signal is not only shifted in location, but is also different in size because the dark spin lies at a different depth than the NV sensor, and magnetic-field gradients along the z -direction are strong compared to the lateral gradients. To achieve high-precision spin-localization in the lateral dimensions, we fit the centre of mass of the measured dark-spin PSF and compared this PSF to the centre of the response circle, yielding the lateral offset $\Delta x = 4.0 \pm 0.4$ nm. The 3D location of this coherently coupled dark spin relative to the NV sensor is illustrated in the cartoon in Fig. 4d. As an additional example, Fig. 4e displays an x - y -plane NV-MRI image of another dark spin that is coherently coupled to a different NV spin (Supplementary Fig. 10). The lateral spatial resolution in this image is 0.8 ± 0.4 nm, and we observe that its location is consistent with being potentially at the diamond surface.

Our NV-MRI demonstration provides the first three-dimensional spatial mapping of dark electronic spins on and near a diamond surface, achieving subnanometre resolution. We expect that NV-MRI will be applicable to a wide range of systems in both the physical and life sciences that can be placed on or near the diamond surface and then probed under ambient conditions. For example, one-dimensional spin chains have been proposed as a method for transferring quantum information²⁸. A key technical challenge that NV-MRI could address is determining the precise

(atomic-scale) location of spins along a chain, which critically influences the fidelity of quantum information transfer. Additionally, individual paramagnetic electron spins with long coherence times at room temperature have attracted interest as potential quantum bits²⁹, but currently such spins cannot be read out individually. NV-MRI would allow for simultaneous control and detection of dark electron spins brought into proximity to NV sensors near the diamond surface. Finally, NV-MRI could image the location of individual electronic spin labels in biological systems^{30,31}, which could aid in determining the structure of proteins.

Furthermore, studying the nanoscale electronic environment on and near diamond surfaces is critical for understanding and maximizing the coherence of NV sensors and quantum bits. We find that the majority of dark spins near shallow NV centres are at the diamond surface and thus we expect that passivation of the surface to reduce the dark-spin density will improve NV-based sensing and quantum information applications. Alternatively, dark spins at the surface could be initialized with NV-assisted spin-polarization techniques^{32,33} and then used as a resource for improved sensing: such ancilla sensor spins would effectively amplify magnetic signals³⁴ from samples placed on^{12,14} or scanned^{10,21} over the diamond surface. In addition, coherently coupled dark spins, which we identified and imaged, can potentially be entangled with the NV sensor to achieve Heisenberg-limited sensing³⁵, thus dramatically increasing metrology performance.

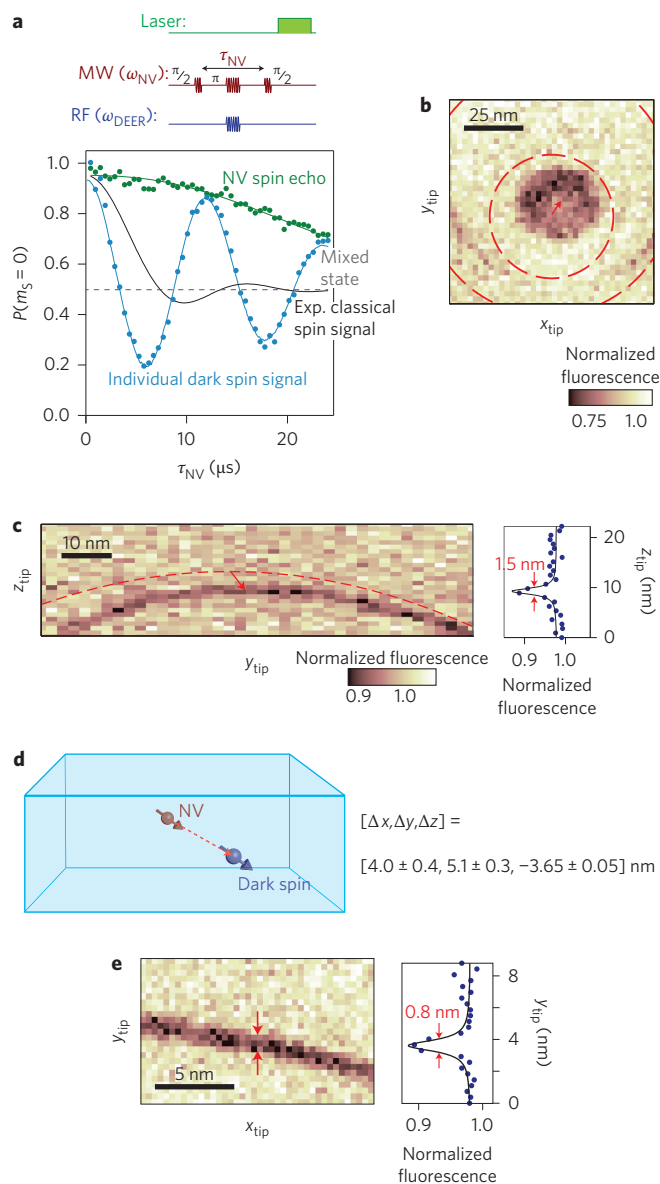


Figure 4 | Individual dark-spin MRI. **a**, Coherent dynamics from an individual dark spin strongly coupled to a single shallow NV centre. Measured oscillations in the NV DEER signal (pulse sequence shown at the top) as a function of spin evolution time τ_{NV} . The DEER signal oscillates coherently and overshoots the NV mixed state, indicated strong coupling of the NV to a single nearby dark electronic spin. For comparison, the expected DEER signal is plotted (black solid line) for comparably strong NV coupling to a single classical spin, demonstrating that the dark-spin effect on the NV DEER signal originates from quantum-projection noise. **b**, Lateral (xy) NV-MRI of a single, coherently coupled dark spin at 50 nm z -axis tip offset; the dark-spin PSF is illustrated in dashed red lines. The vector connecting the centre of the PSF circle and the dark-spin resonance gives the lateral shift (Δx , Δy) of the dark spin from the NV. Two distinct resonant slices appear because different sets of dark-spin hyperfine transitions (Supplementary Figs 7 and 8) are driven by the applied RF signal. **c**, Vertical (yz) NV-MRI of the same coherently coupled dark spin as shown in **b**. Scanning the magnetic tip across the symmetry plane of the lateral image in **b** gives the dark-spin vertical shift Δz , in addition to a second measure of Δy . The tip-induced magnetic-field gradient along the z -direction provides 1.5 nm spatial resolution. **d**, Illustration of the three-dimensional location of the coherently coupled dark spin relative to the NV sensor, as determined from data in **b** and **c**. **e**, Lateral (xy) NV-MRI of a second coherently coupled dark spin, imaged with 0.8 nm resolution.

Received 22 October 2013; accepted 27 January 2014; published online 23 March 2014

References

- Mansfield, P. Snapshot magnetic resonance imaging (Nobel lecture). *Angew. Chem. Int. Ed.* **43**, 5456–5464 (2004).
- Glover, P. & Mansfield, P. Limits to magnetic resonance microscopy. *Rep. Prog. Phys.* **65**, 1489–1511 (2002).
- Palma, C.-A. & Samori, P. Blueprinting macromolecular electronics. *Nature Chem.* **3**, 431–436 (2011).
- Cai, J., Retzker, A., Jelezko, F. & Plenio, M. B. A large-scale quantum simulator on a diamond surface at room temperature. *Nature Phys.* **9**, 168–173 (2013).
- Sidles, J. A. *et al.* Magnetic resonance force microscopy. *Rev. Mod. Phys.* **67**, 249–265 (1995).
- Balasubramanian, G. *et al.* Nanoscale imaging magnetometry with diamond spins under ambient conditions. *Nature* **455**, 648–651 (2008).
- Degen, C. L., Poggio, M., Mamin, H. J., Rettner, C. T. & Rugar, D. Nanoscale magnetic resonance imaging. *Proc. Natl Acad. Sci. USA* **106**, 1313–1317 (2009).
- Rugar, D., Budakian, R., Mamin, H. J. & Chui, B. W. Single spin detection by magnetic resonance force microscopy. *Nature* **430**, 329–332 (2004).
- Grinolds, M. S. *et al.* Quantum control of proximal spins using nanoscale magnetic resonance imaging. *Nature Phys.* **7**, 687–692 (2011).
- Maletinsky, P. *et al.* A robust scanning diamond sensor for nanoscale imaging with single nitrogen-vacancy centres. *Nature Nanotech.* **7**, 320–324 (2012).
- Grotz, B. *et al.* Sensing external spins with nitrogen-vacancy diamond. *New J. Phys.* **13**, 055004 (2011).
- Mamin, H. J. *et al.* Nanoscale nuclear magnetic resonance with a nitrogen-vacancy spin sensor. *Science* **339**, 557–560 (2013).
- Mamin, H. J., Sherwood, M. H. & Rugar, D. Detecting external electron spins using nitrogen-vacancy centers. *Phys. Rev. B* **86**, 195422 (2012).
- Staudacher, T. *et al.* Nuclear magnetic resonance spectroscopy on a (5 nm)³ sample volume. *Science* **339**, 561–563 (2013).
- Steinert, S. *et al.* Magnetic spin imaging under ambient conditions with sub-cellular resolution. *Nature Commun.* **4**, 1607 (2013).
- Ermakova, A. *et al.* Detection of a few metallo-protein molecules using color centers in nanodiamonds. *Nano Lett.* **13**, 3305–3309 (2013).
- Gruber, A. *et al.* Scanning confocal optical microscopy and magnetic resonance on single defect centers. *Science* **276**, 2012–2014 (1997).
- De Lange, G. *et al.* Controlling the quantum dynamics of a mesoscopic spin bath in diamond. *Sci. Rep.* **2**, 382 (2012).
- Larsen, R. G. & Singel, D. J. Double electron–electron resonance spin-echo modulation: spectroscopic measurement of electron spin pair separations in orientationally disordered solids. *J. Chem. Phys.* **98**, 5134–5146 (1993).
- Schoenfeld, R. S. & Harneit, W. Real time magnetic field sensing and imaging using a single spin in diamond. *Phys. Rev. Lett.* **106**, 030802 (2011).
- Grinolds, M. S. *et al.* Nanoscale magnetic imaging of a single electron spin under ambient conditions. *Nature Phys.* **9**, 215–219 (2013).
- Ofori-Okai, B. K. *et al.* Spin properties of very shallow nitrogen vacancy defects in diamond. *Phys. Rev. B* **86**, 081406 (2012).
- Ohno, K. *et al.* Engineering shallow spins in diamond with nitrogen delta-doping. *Appl. Phys. Lett.* **101**, 082413 (2012).
- Dolde, F. *et al.* Room-temperature entanglement between single defect spins in diamond. *Nature Phys.* **9**, 139–143 (2013).
- Tetienne, J. P. *et al.* Spin relaxometry of single nitrogen-vacancy defects in diamond nanocrystals for magnetic noise sensing. *Phys. Rev. B* **87**, 235436 (2013).
- McGuinness, L. P. *et al.* Ambient nanoscale sensing with single spins using quantum decoherence. *New J. Phys.* **15**, 073042 (2013).
- Shi, F. *et al.* Quantum logic readout and cooling of a single dark electron spin. *Phys. Rev. B* **87**, 195414 (2013).
- Yao, N. Y. *et al.* Robust quantum state transfer in random unpolarized spin chains. *Phys. Rev. Lett.* **106**, 040505 (2011).
- Harneit, W. Fullerene-based electron-spin quantum computer. *Phys. Rev. A* **65**, 032322 (2002).
- Altenbach, C., Marti, T., Khorana, H. & Hubbell, W. Transmembrane protein structure: spin labeling of bacteriorhodopsin mutants. *Science* **248**, 1088–1092 (1990).
- Kaufmann, S. *et al.* Detection of atomic spin labels in a lipid bilayer using a single-spin nanodiamond probe. *Proc. Natl Acad. Sci. USA* **110**, 10894–10898 (2013).
- Belthangady, C. *et al.* Dressed-state resonant coupling between bright and dark spins in diamond. *Phys. Rev. Lett.* **110**, 157601 (2013).
- Laraoui, A. & Meriles, C. A. Approach to dark spin cooling in a diamond nanocrystal. *ACS Nano* **7**, 3403–3410 (2013).

34. Schaffry, M., Gauger, E. M., Morton, J. J. L. & Benjamin, S. C. Proposed spin amplification for magnetic sensors employing crystal defects. *Phys. Rev. Lett.* **107**, 207210 (2011).
35. Goldstein, G. *et al.* Environment-assisted precision measurement. *Phys. Rev. Lett.* **106**, 140502 (2011).

Acknowledgements

The authors thank S. Kolkowitz, N. de Leon and C. Belthangady for technical discussions regarding optimizing NV-based sensors and M. Markham and Element Six for providing diamond samples. The authors acknowledge discussions on the detection of dark spins using DEER with M. D. Lukin, A. Sushkov, I. Lovchinsky, N. Chisholm, S. Bennett, and N. Yao. M.S.G. is supported through fellowships from the Department of Defense (NDSEG programme) and the National Science Foundation. M.W. is supported through a Marie Curie Fellowship and K.D.G. acknowledges support from the Harvard Quantum Optics Center as an HQOC postdoctoral fellow. This work was supported by the DARPA QuEST and QuASAR programmes and the MURI QuISM.

Author contributions

M.S.G., M.W. and A.Y. conceived the basic principles of NV-MRI. M.S.G., S.H., P.M. and A.Y. built the combined atomic force and confocal microscope for NV experiments. M.S.G. and A.Y. performed the experiments and analysed the data with input from all authors. All authors contributed to writing the manuscript.

Additional information

Supplementary information is available in the [online version](#) of the paper. Reprints and permissions information is available online at www.nature.com/reprints. Correspondence and requests for materials should be addressed to A.Y.

Competing financial interests

The authors declare no competing financial interests.